Experimental determination of the partitioning coefficient of β-pinene oxidation products in SOA

SCHOLARONE™
Manuscripts

Journal Name

Dynamic Article Links ▶

ARTICLE TYPE

Experimental determination of the partitioning coefficient of β-pinene oxidation products in SOA

Thorsten Hohaus[a], Iulia Gensch[*,a] , Joel Kimmel[b] , Douglas Worsnop[b] and Astrid Kiendler-Scharr[a]

The composition of secondary organic aerosol (SOA) formed from β-pinene ozonolysis was experimentally investigated in the Juelich aerosol chamber. Partitioning of oxidation products between gas and particles was measured through concurrent concentration measurements in both phases. Partitioning coefficients (K_p) of $2.23 \times 10^{-5} \pm 3.20 \times 10^{-6}$ m^3 μg^{-1} for nopinone, $4.86 \times 10^{-4} \pm 1.80 \times 10^{-4}$ m^3
10 μg^{-1} for apoverbenone, $6.84 \times 10^{-4} \pm 1.52 \times 10^{-4}$ m^3 μg^{-1} for oxonopinone and $2.00 \times 10^{-3} \pm 1.13 \times 10^{-3}$ m^3 μg^{-1} for hydroxynopinone were derived, showing higher values for more oxygenated species. The observed K_p values were compared with values predicted using two different semi-empirical approaches. Both methods led to an underestimation of the partitioning coefficients with systematic differences between the methods. Assuming that the deviation between experiment and model is due to non-ideality of the mixed
15 solution in the particles, activity coefficients of 4.82×10^{-2} for nopinone, 2.17×10^{-3} for apoverbenone, 3.09×10^{-1} for oxonopinone and 7.74×10^{-1} for hydroxynopinone would result using the vapour pressure estimation technique that leads to higher K_p . We discuss that such large non-ideality for nopinone could arise from particle phase processes lowering the effective nopinone vapour pressure such as diol- or dimer formation. The observed high partitioning coefficients compared to modelled results imply an
20 underestimation of SOA mass by applying equilibrium conditions.

Introduction

Ozonolysis of monoterpenes is an important source of atmospheric secondary organic aerosol (SOA)[1, 2]. The partitioning of the semi-volatile oxidation products between gas
25 and particle phase represent a key process in the SOA formation and evolution, yet is poorly described in the regional and global atmospheric models[3-5]. Representations of the gas-phase chemistry leading to oxygenated semi-volatile and low-volatile species use near-explicit oxidation mechanisms of volatile
30 organic compound (VOC), e.g. the Master Chemical Mechanism (MCM 3.1, http://mcm.leeds.ac.uk/MCM,[6]). These mechanisms can, at best, describe the first oxidation steps, and higher or oxidation steps have to be parameterized. To simulate SOA formation, chemical modules can be coupled to a partitioning
35 module. It is typically assumed that the organic compounds partition between gaseous and condensed phase as a function of their vapour pressure[7, 8]. Laboratory measurements are technically difficult in the low vapour pressure range, let alone they cannot cover the large diversity of the semi-volatile and low-
40 volatile oxidation products. Moreover, SOA are complex non-ideal mixtures of different chemical components with different energetic interactions. Under humid conditions, deviations from equilibrium conditions due to the non-ideality become more important[7, 9]. Water uptake in the aerosol might imply an increase
45 in the particulate concentration of semi-volatile water soluble species.

Vapour pressure estimations typically vary over several orders of magnitude[10 and references therein]. Together with uncertainties in activity coefficients due to simplifying assumptions in the
50 thermodynamics of mixed organic-inorganic aerosols, these estimates contribute to large uncertainties in the assessment of total global SOA production (e.g.[5, 11-14]). Therefore, more SOA formation experiments are needed for identification and quantification of oxidation products in gas and particle phase[15, 16].
55 The first goal of this study was to experimentally determine the partitioning coefficient of several semi-volatile SOA components. Therefore, simultaneous gas and particle phase measurements of organic compounds arising during the dark ozonolysis of β-pinene were carried out in the Juelich aerosol chamber. High
60 mass resolution information derived from Proton Transfer Reaction Time of Flight Mass Spectrometer (PTR-ToF-MS,[17]) data ensured accurate identification and distinction of isobaric gas phase compounds having the same m/z. The particle phase was characterized using the Aerosol Collection Module coupled to a
65 Gas Chromatograph with a Flame Ionization Detector - Mass Spectrometer system (ACM GC-MS,[18]).

The measured partitioning coefficients were compared with the estimated values, obtained by employing semi-empirical vapour pressure formulations derived from the Clausius-Clapeyron
70 equation, together with thermodynamical data predicted from molecular structure of the investigated organic compounds.

Equilibrium partitioning formalism

The partitioning of organic semi-volatile species between gas and particulate phase represents the fraction of a single compound i in the condensed phase relative to the amount of i in the gas phase
5 normalized by the total organic particulate mass and can be described by an equilibrium partitioning coefficient $K_{p,i}$ [12, 19]:

$$\frac{C_i^p}{C_i^g} = K_{p,i} \cdot C_{OA} \tag{1}$$

where $K_{p,i}$ represents the equilibrium partitioning coefficient [m³ μg⁻¹], C_i^p and C_i^g are mass concentrations of species i per unit
10 volume air in the particulate and gas phase, respectively [μg m⁻³] and C_{OA} gives the mass concentration of total absorbing particulate phase per unit volume air [μg m⁻³].

According to the currently employed absorption equilibrium partitioning formalism, K_p can be thermodynamically expressed
15 as [20, adapted from 21]:

$$K_{p,i} = \frac{7.501 \cdot 10^{-9} \cdot R \cdot T}{MW_{OM} \cdot \zeta_i \cdot p_{L,i}^0} \tag{2}$$

where R is the ideal gas constant [J mol⁻¹ K⁻¹], T the temperature [K], MW_{OM} the mean molar weight of the condensed organic phase [g mol⁻¹], ζ_i the activity coefficient for the given species in
20 the condensed organic phase [1] and $p_{L,i}^0$ the sub-cooled liquid vapour pressure [Torr].

From a thermodynamics point of view, the activity coefficient represents the non-ideality of a semi-volatile compound which is dissolved in the organic fraction of the particle. The activity
25 coefficient changes with the composition of the organic part of the particles. For simplicity, in most studies and models, it is assumed that ζ_i is unity for an oxidized product, which partitions into an aerosol composed of a mixture of similar compounds[22]. Nevertheless, the activity coefficients of organic compounds
30 representing the majority of atmospheric SOA are considered to lie in the range of 0.3 to 3[23].

To estimate $K_{p,i}$, knowledge of sub-cooled liquid vapour pressure is necessary. Yet, experimental information is scarce and no analytical method is currently available to calculate $p_{L,i}^0$ and its
35 temperature dependence from theory alone. Therefore, different empirical and semi-empirical relations were developed by integrating the Clausius-Clapeyron equation and making simplifying assumptions on the missing information. Depending on these assumptions, the predicted thermodynamic properties
40 can show significant differences. In a study on α-pinene ozonolysis, Camredon et al.[24] reported a divergence of 3 to 5 orders of magnitude in $p_{L,i}^0$ calculations for "top ten" species found to have a dominant contribution to SOA formation, when using different approaches.
45 Here, we apply the two $p_{L,i}^0$ estimation methods presented by Camredon et al.[24], giving the lowest and highest vapour pressures. First, the Myrdal and Yalkowsky[25] $p_{L,i}^0$ semi-empirical equation was combined with the Joback and Reid[26] molecular predictions of boiling points, T_B. This method (further referred to
50 as Camredon's method) is considered to underestimate vapour pressures[27]. Contrarily, Jenkin[20] recommends applying a scaling-up factor of two orders of magnitude to the rate constants for gas/particle partitioning to be able to simulate the measured

experimental data. This translates into a significant
55 overestimation of $p_{L,i}^0$. For vapour pressure calculations, the author employed a modified form of the Mackay $p_{L,i}^0$ semi-empirical equation[28] coupled with the Stein and Brown structure depending estimates for boiling points[29]. This approach will be further referred to as Jenkin's method. T_B values are estimated in
60 both cases as functional group contribution methods by summing the contributions multiplied by the number of the functional groups in the given compounds. Compared to Stein and Brown, the Joback and Reid data set explicitly contains ring increments, which are relevant for monoterpene calculations. Further,
65 contrary to Mackay et al., who assume that the heat capacity changes for phase transitions are negligible, Myrdal and Yalkowsky include these differences into their empirical equation to estimate $p_{L,i}^0$. Moreover, the authors account for hydrogen bonding effect in the boiling entropy term, thus eliminating errors
70 in estimating the vapour pressure of complex organic compounds.

Experimental section

The experiment was carried out under dark conditions at atmospheric pressure in the Forschungszentrum Juelich (FZJ) 260 m³ aerosol chamber. This facility has been previously
75 described by Mentel et al.[30]. Prior to the experiment, the chamber was flushed with particle free air. After flushing, the initial conditions inside the chamber were 27 % relative humidity, a temperature of 20 ºC, and an ozone con-centration of approximately 20 ppb. The particle number concentration was
80 lower than 20 cm⁻³. As representative of common monoterpenes emitted from terrestrial vegetation, 583 ppbv β-pinene (Aldrich, 99% purity) were introduced into the chamber. The reaction started after injecting an excess of ozone (1ppm of ozone, 99.998 % purity). Secondary organic aerosol (SOA) particles formed
85 immediately. The high concentration of the gas phase precursors was used to ensure sufficient aerosol mass in the beginning of the reaction. Moreover, the excess of ozone aimed the full consumption of β-pinene during the time of the experiment. Since no OH-scavenger was used, the reaction was to some extend
90 affected by an additional oxidation by OH radicals[31].

Temperature, relative humidity, pressure, ozone concentration, aerosol concentration (Condensation Particle Counter (CPC), TSI3786), and aerosol size distribution (Scanning Mobility Particle Sizer (SMPS), TSI3934) inside the aerosol chamber were
95 permanently monitored during the experiment. For the purpose of this study, gas phase precursor and oxidation products were measured by PTR-ToF-MS (Ionicon, Innsbruck, Austria[17]). The aerosol chemical composition was acquired with the Quadrupole Aerosol Mass Spectrometer (AMS, Aerodyne Research, Billerica,
100 USA[32, 33]). Additionally, the particle phase composition was obtained with the ACM GC-MS[18]. Further details on sampling, analysis procedures and experimental details were described previously[18].

Gas phase measurements of VOC utilized ionization by proton
105 transfer reaction. The use of the PTR-Tof-MS[17] allowed for high mass resolution (~4000) making the identification of isobaric ions on same nominal mass possible. Peak integration used a custom function to account for deviations of actual peak shape from Gaussian peaks as established for high mass resolution aerosol
110 mass spectrometry. Peak fitting uses a list of user-defined

possible ions at pre-defined exact m/z positions while minimizing the residual signal [34]. Gas phase concentration measurements of β-pinene and nopinone were calculated using known fragmentation patterns[35-37] and a proton transfer reaction rate coefficient of $2.5 \cdot 10^{-9}$ cm^3 s^{-1} for β-pinene[38]. The quantification of apoverbenone, oxonopinone, and hydroxynopinone assumes the same fractional contribution of the parent ion to total signal as for nopinone. Note that in the absence of authentic standards and without determination of potential fragmentation processes, the gas phase concentration measurement error is on the order of 30%.

AMS measurements were performed to quantify the total organic mass and determine typical mass spectra of the SOA formed. Based on the AMS measurements, inorganic contributions to the observed particle mass could be excluded. AMS data analysis utilized standard procedures[39], adapting the fragmentation table to the chamber conditions. A positive matrix factorization (PMF) analysis was performed on the AMS mass spectra[40]. Three characteristic factors were identified with distinct temporal evolution during the course of the experiment.

The ACM GC-MS system has been described in detail elsewhere[18]. In brief, aerosol particles are focused into a narrow particle beam using an aerodynamic lens system[41, 42]. Inside the lens, gas phase species are removed from the sample volume and the particle beam passes subsequently through a vacuum chamber and impacts onto a small chemically passivated (Silcosteel, SilcoTek, Bellefonte, PA), cooled sampling surface. The sampling flow is 80 ml/min. After one sampling episode is completed, the particles are desorbed from the collection surface and transferred via a carrier gas (helium with a minimum purity of 99.9999%) into the GC/FID-MS detector for analysis. The collection time for each ACM GC-MS sample was 60 min. The collection temperature of the collector was -30 °C and the desorption temperature 225 °C. The aerosol sample was desorbed for 6 min from the collector. The volatilized mixture was transferred to a Fission8060 Gas Chromatograph equipped with a DB-5ms capillary column (60 m x 0.25 mm ID, film thickness 0.25 μm, J&W Scientific, Folsom, USA). The chromatographically separated compounds were detected in parallel with a Flame Ionization Detector (FID) and a FisionMD800 Quadrupole Mass Spectrometer (MS). In total 16 ACM GC-MS measurements (thereunder a blank before injecting the reactants) with a 60 min sampling interval were carried out over a time period of 57 hours after the reaction start. The ACM GC-MS system shows good linearity in the range of 10 to 100 ng investigated particulate mass, with an overall measurement error of up to 10%.

Results and discussions

Gas Phase Measurements

Exploiting the high resolution capabilities of the PTR-TOF-MS, an ion at the nominal mass m/z 137 was detected, interfering with the parent β-pinene signal itself. The exact mass determination revealed that the sum formula was $C_9H_{12}OH^+$, the ion being identified as the protonated 6,6-dimethyl-bicyclo[3.1.1]hept-3-en-2-one (apoverbenone), i.e. an oxidation product of β-pinene[43].

Figure 1 illustrates clear signals of both β-pinene and apoverbenone, at m/z 137.1330 and 137.0966, respectively. While the β-pinene signal is very strong in the beginning of the reaction, after four hours, the apoverbenone became the dominant component.

Fig. 1 Temporal evolution of the signal detected at m/z 137, showing an increasing contribution of the peak at m/z 137.0966 (bicyclo[3.1.1]hept-3 en-2-one, 6,6-dimethyl - apoverbenone – orange line) with increasing time. The β-pinene (black line) at m/z 137.1330 is largest in the beginning of the experiment, when ozone and β-pinene were injected into the chamber.

The time series of gas phase concentration of β-pinene and four of its oxidation products (Fig. 2) show that β-pinene was almost entirely consumed within four hours from the start of the experiment. Selection criteria for the gas phase oxidation products presented here were the high concentration detected and accurate chemical speciation. The concentration of apoverbenone exhibited similar behavior as the nopinone concentration, increasing steeply at the beginning of the experiment. Six hours after the reaction start, the concentration of both oxidation products reached their maxima, afterwards decreasing continuously. Due to the double bound, it is very likely that apoverbenone further reacted with ozone, resulting in a steeper drop of its concentration compared to nopinone. The concentration of higher oxidized products hydroxynopinone and oxonopinone increased slowly during the first 12 hours.

Fig. 2 Temporal evolution of gas phase concentration of β-pinene (m/z 137.1330, black line), nopinone (m/z 139.1123, green line), apoverbenone (m/z 137.0966, orange line), oxonopinone (m/z 153.0916, blue line), and hydroxynopinone (m/z 155.1072, red line) during the experiment.

In order to better interpret the measurements and the instrument performances, the temporal evolution of precursors and ozonolysis products was simulated by using the MCM. Parts of the mechanism were extracted by selecting β-pinene as primary VOC and its initial degradation products. According to the simulations, the concentration of nopinone increases during the first five and a half hours to its maximum of 271 ppb and remains constant. This behavior is due to the fact that MCM treats only the gas phase reactions, neglecting the partitioning of semi volatile compounds into aerosol particles. The maximum total measured nopinone concentration was 172 ppb, representing 0.64 of the simulated value. Within instrumental error range, and considering the loss processes in the chamber, the formation of the major product of the β-pinene ozonolysis was fairly well described by the model.

Temporal Evolution of β-pinene SOA composition

The mass concentration of specific organic compounds in the aerosol was measured by ACM-GC-MS. Further, their masses were normalized to the collector mass loading determined from the SMPS measurements[18]. Figure 3 shows the particle phase concentrations of β-pinene oxidation products for the 15 sampling episodes. Similar to observations in the gas phase nopinone decreases throughout the experiment. The temporal

evolution of the other particle phase components is less pronounced.

Fig. 3 Concentrations of nopinone (green), apoverbenone (orange), oxonopinone (blue), and hydroxynopinone (red) in the particulate phase
5 for the ACM sampling episodes.

As mentioned above, the overall organic aerosol mass concentration was also measured by an AMS throughout the experiment. The mass spectral evolution of the SOA was evaluated by a PMF analysis of the data set, showing that the
10 total organics could be described by three factors. Figure 4 depicts the factors normalized to the total organic mass measured with the AMS. While factor 1 (green line) shows a steady decrease, factor 2 (blue line) reaches its maximum after 10.5 hours and decreases afterwards. Factor 3 (red line) increases even
15 slower, but continuously.

The mass spectra of the individual factors indicated differences in the relative contributions of ions at m/z 27 to 29, 41 to 44, and 55. The relative oxygen content in organic aerosol was estimated using the fraction of the organic signal at m/z 44[44]. From the
20 PMF analysis, O/C ratios of 0.403, 0.121 and 0.286 were derived for the AMS factors 1, 2 and 3, respectively.

Pearson correlation analyses were carried out between temporal trends of mass fractional abundances derived from ACM-GC-MS measurements and the factors determined from the PMF analysis
25 of the AMS data. Most correlation coefficients were statistically significant (p-value <0.05), but to different degree. Accordingly, the organic compounds measured by ACM-GC-MS could be sorted in three categories, each of them reproducing an AMS-PMF factor in its time evolution. From 46 identified peaks, 26
30 organic compounds showed strong correlation with factor 1 (green line), 3 with factor 2 (blue line) and 10 with factor 3 (red line). The time series of particle phase concentrations of nopinone and apoverbenone match the evolution of PMF factor 1, while the time series of particle phase concentration of oxonopinone and 1-
35 hydroxynopinone follow the factors 2 and 3, respectively.

Fig. 4 AMS factors (green, blue and red solid lines for AMS factors 1, 2 and 3, respectively), from PMF analysis vs. total fractional abundances of the ACM factors. The ACM factors (green, blue and red dashed lines for
40 ACM factors 1, 2 and 3, respectively) were obtained by adding the contributions of all peaks, which could be assigned to a specific time evolution (for details, see text). Stars represent the sum of the peak contributions.

The contributions of all identified and non-identified organic
45 compounds were summed for each category, being then translated into ACM factors 1 to 3 (dashed lines, green, blue and red, respectively), corresponding to the PMF factors. For both, the PMF factors and the ACM factors, factor 1 is the dominant factor in the early stage of the experiment. However the drop of
50 the PMF factor 1 is more pronounced than the ACM factor 1. A significant difference appears in the contribution of the ACM factors 2 and 3 compared to the corresponding PMF factors. While the PMF factor 2 contribution to the total mass is up to 50%, the ACM factor 2 only gives 10%. Moreover, twelve hours
55 after the start of the reaction, the contribution of the ACM factor 3 becomes higher than that of ACM factor 2, in contrast to the evolution of the corresponding PMF factors which show roughly

equal contributions by the end of the experiment. These differences indicate that, despite the identical source of SOA
60 sampling for both setups, the detection efficiency for different compounds or compound classes is not the same for the two instruments. Compounds which were measured by the AMS and contributed to the increase of PMF factors 2 and 3 could not be fully detected by ACM-GC-MS. These might be compounds such
65 as polar highly oxidized species or generally higher molecular weight compounds. This is also in line with a comparison of the O/C ratios calculated from the AMS mass spectral fingerprints and from ACM-GC-MS observed individual compounds. ACM-GC-MS compounds have an O/C ratio of 0.11 (nopinone and
70 apoverbenone) compared to 0.40 of the PMF factor 1, 0.22 (oxonopinone) compared to 0.12 of PMF factor 2 and 0.22 (hydroxynopinone) compared to 0.29 of PMF factor 3. The result of this comparison is ambiguous. While the O/C ratio of hydroxynopinone is within the scope of the O/C ratio of factor 3,
75 the comparison for factors 1 and 2 is inconclusive.

Partitioning of β-pinene ozonolysis products

The partitioning coefficients of nopinone, apoverbenone, oxonopinone and hydroxynopinone were determined from PTR-
80 ToF-MS, SMPS, and ACM-GC-MS data using Equation 1. The results are presented in Figure 5.

Fig. 5 Time series of the partitioning coefficients of nopinone (green), apoverbenone (orange), oxonopinone (blue), and hydroxynopinone (red).

85 In most cases the measured partitioning coefficients stayed nearly constant during the experiment, showing values of $2.23 \cdot 10^{-5} \pm 3.20 \cdot 10^{-6}$ m µg^{-3} for nopinone, $4.86 \cdot 10^{-4} \pm 1.80 \cdot 10^{-4}$ m µg^{-3} for apoverbenone, $6.84 \cdot 10^{-4} \pm 1.52 \cdot 10^{-4}$ m µg^{-3} for oxonopinone and $2.00 \cdot 10^{-3} \pm 1.13 \cdot 10^{-3}$ m µg^{-3} for hydroxynopinone. The fact that
90 nopinone partitioning coefficient for the first sample, i.e. 1.3 hours after ozone was injected, is significantly different from those measured later in the experiment can be explained by changes in the composition in the SOA during the ongoing reaction in the chamber. In the first four hours, most of the ozone
95 reacts with the compounds, so that the composition of the SOA continuously changes, undergoing an increase of newly formed low- and semi-volatile oxygenated products from the β-pinene ozonolysis. Therefore the conditions for the first generation products to partition into the SOA could change and accordingly,
100 the partitioning coefficients would change. However, the time resolution of sampling, especially at the beginning of the experiment, was too low to give any further insight into the very dynamical processes occurring in this time period of highest reactant consumption in the chamber.
105 The compound specific standard deviations presented above for the partitioning coefficients must be combined with errors describing the accuracy and precision of the measuring instruments. Sources of these systematic errors might be the under sampling of semi volatile species by the ACM system
110 (10%), if these evaporate under the low pressure collection conditions. As for gas phase concentration- measurements using PTR-MS, these are dominated by uncertainties due to fragmentation of the targeted compounds. The systematic error

was 30-50%, with higher values for the non-calibrated species (apoverbenone, oxonopinone and hydroxynopinone). The uncertainty in measuring total suspended particulate mass concentration by the SMPS system was 20-50%. Overall, an
5 uncertainty of 37-71% for partitioning coefficients can arise from measurements errors, with lowest values corresponding to nopinone and highest for the more oxidized compounds.
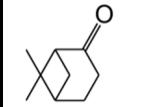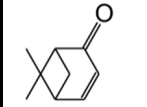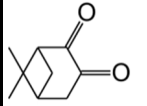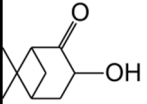
The experimentally obtained values were compared with $K_{p,i}$ derived from Equation 2, using Camredon's and Jenkin's
10 approaches to predict the vapour pressure (see above). The calculations were carried out for 298 K using a mean molar weight for the particle phase organics of 180 g/mol[45] and an activity coefficient ζ_i =1. As shown in Figure 5, $K_{p,i}$s derived experimentally are up to three orders of magnitudes higher than
15 the calculated values, showing better agreement to the values derived from Camredon's approach.

Fig. 6 Comparison of measured (open bars) with predicted partitioning coefficients for nopinone (green), apoverbenone (orange), oxonopinone

20 (blue), and hydroxynopinone (red). The estimated values are derived accordingly to Camredon's (stripped bars), respectively Jenkin's method (filled bars).

Table 1 provides an outline of the comparison of the observed partitioning coefficients with the predicted values, which were
25 obtained by employing Jenkin's, respectively Camredon's approach to estimate the sub-cooled vapour pressure of nopinone, apoverbenone, oxonopinone and hydroxynopinone. The mean K_p values were calculated by excluding the first sampling point, since the aerosol system has not reached its equilibrium 1.3 h
30 after the reaction had started. Additionally, predicted activity coefficients for the investigated species are presented for the assumption that the discrepancy between experiment and theory arises from the non-ideality of the solutions in the aerosol particles. Excepting the values corresponding to the higher
35 oxidized compounds oxonopinone and hydroxynopinone, if derived from Camredon's calculations, the ζ_i are several orders of magnitude lower than those suggested in the literature.

Table 1 Observed and predicted (for detail see text) partitioning coefficients of nopinone, apoverbenone, oxonopinone and hydroxynopinone, O/C ratios, as well as activity coefficients emerged from the assumption that deviation between experiment and model is due to the non-ideality of the mixed solution in the particles.

Name	Chem. structure	O/C	Exp. K_p $m^3\ \mu g^{-1}$	Predicted K_p ($\zeta_i = 1$) $m^3\ \mu g^{-1}$		Predicted ζ_i	
				Meth. Jenkin	Meth. Camredon	Meth. Jenkin	Meth. Camredon
Nopinone $C_9H_{14}O$		0.15	2.23×10^{-5}	3.08×10^{-7}	1.08×10^{-6}	1.38×10^{-2}	4.82×10^{-2}
Apoverbenone $C_9H_{12}O$		0.15	4.86×10^{-4}	4.10×10^{-7}	1.06×10^{-6}	8.26×10^{-4}	2.17×10^{-3}
Oxonopinone $C_9H_{12}O_2$		0.30	6.84×10^{-4}	1.34×10^{-6}	2.12×10^{-4}	1.96×10^{-3}	3.09×10^{-1}
Hydroxynopinone $C_9H_{14}O_2$		0.30	2.00×10^{-3}	3.04×10^{-5}	1.68×10^{-3}	1.52×10^{-2}	7.74×10^{-1}

Possible sources of the differences shown in Figure 6 and Table 1 might arise either from instrumental errors, or from inaccurate
40 assumptions on the mean molar weight of the condensed organic phase MW_{OM} , on the activity coefficients ζ_i , or on the sub-cooled liquid vapour pressure $p^0_{L,i}$. As stated above, experimental errors are in the range 37–71 %, too low to account for the observed differences. Further, experimental errors should lead to
45 largest biases in the higher oxidized substances. For nopinone, which shows the largest disagreement between measured and calculated $K_{p,i}$, it is also worth mentioning that observed gas phase nopinone is in reasonable agreement with the MCM excluding experimental errors to the extent required to reconcile
50 with calculated $K_{p,i}$ values. Comparing the MW_{OM} used in the calculations with aerosol typical values (180-200 g mol^{-1}), the

possibility of an overestimation of this term by a factor of at least 20 can be excluded too. Having covered a broad range of $p^0_{L,i}$ we further explore to what extent activity coefficients deviating from
55 1 can explain observed differences.

To this end, composition dependent activity coefficient calculations were carried out using the thermodynamic group-contribution model AIOMFAC (e.g.[46]). This approach accounts for the non-ideality of the interactions among organic functional
60 groups and between organic functional groups and water in the aerosol. To initialize the model, a multicomponent solution containing water and organic compounds was defined. The organic mixture was defined to consist of the most abundant degradation products of the β-pinene ozonolysis derived from the
65 MCM simulations, likely contributing to the condensed material.

Beside nopinone, oxonopinone and hydroxynopinone, eight other compounds were considered, containing different functional groups, such as hydroxyl, carboxyl, ketone, aldehyde, hydrogen peroxide and water. The mass contribution of individual components was calculated to provide self-consistent composition with the PMF factors found from AMS measurements and their corresponding O/C ratios. The mass fraction of water in the mixture was varied, so that the estimated relative humidity matched the experimental one. For nopinone, oxonopinone and hydroxynopinone activity coefficients of 2.50 ± 0.20, 2.30 ± 0.08 and 0.98 ± 0.11 respectively were determined, showing a strong discordance with the predicted values for absorptive partitioning (Table 1).

This suggests that the gas-particle partitioning of semi-volatile organic compounds such as nopinone cannot be described just by using the absorption equilibrium formalism. Similar observations were made by[47], who showed an irreversible, kinetically determined uptake of nitrates on existing particles during the oxidation of α-pinene by NO_3 radicals. For nopinone we suggest too, that non-equilibrium processes drive the balance towards its uptake from the gas into the particulate phase. A possible explanation might be that once absorbed into aerosol, nopinone is bound in form of very low volatile compounds, such as ketone-hydrates (diols) or ketone-dimers, with vapour pressures some orders of magnitude lower than that of the precursor ketone. These presumed compounds could show thermal instability during the thermal desorption step in the ACM-GC-MS, releasing nopinone during the measurements.

Summary and Conclusions

A β-pinene ozonolysis experiment, with no OH scavenger, was carried out in the Juelich aerosol chamber under dark conditions, to investigate SOA formation. Oxidation products were identified and their concentrations were measured in gas and particle phase, using high resolution PTR-Tof-MS, respectively an ACM GC-MS. Detailed analyses were accomplished for four abundant components. Nopinone was confirmed to be the major oxidation product, showing concentrations of one to two orders of magnitude higher than apoverbenone, oxonopinone and hydroxynopinone. The increase in the gas phase concentration in the beginning of the experiment was smoother for the higher oxidized species; e.g. hydroxynopinone increased during the first twelve hours contrary to nopinone which reached its maximum after six hours. The subsequent decreasing of concentration was steeper for apoverbenone, which, due to the double bond, might further have reacted with ozone. β-Pinene was consumed in the first four hours of the reaction. The temporal evolution of the ozonolysis products in particle phase showed also different behavior of the species containing one against those with two oxygen atoms in the molecule. Other than nopinone and apoverbenone, which mainly decreased during the experiment, oxonopinone and hydroxynopinone concentrations showed an increasing tendency even after complete β-pinene depletion.

Based on the absorption equilibrium partitioning formalism, K_p was derived from simultaneously obtained gas and particle phase concentration data, showing values between $2.23 \cdot 10^{-5}$ and $2.00 \cdot 10^{-3}$ m µg^{-3}. This compares with another nopinone partitioning experimental study by Khant[48], who reported a K_p of $1.1 \cdot 10^{-4}$ - $2.4 \cdot 10^{-4}$. The higher oxidized compounds showed higher partitioning in the aerosol phase, which implies that adding oxygen in the course of reaction lowers the volatility, in agreement with theory. [49] estimate a similar high partitioning for nopinone, deriving K_p from fitting model results to experimental determination of the overall SOA yield in a smog chamber. The calculations, aimed to be implemented in global modelling, use a weighted fit algorithm developed by [2, 50], basing on a narrow set of chemical reactions describing β-pinene oxidation by OH, O_3 and NO_3. The authors caution that considerable uncertainty remains in employing this method to determine the partitioning coefficients for single compounds.

Additionally, K_p was calculated by using vapour pressure data predicted from molecular models. Two different methods were tested against the experimental data, both using semi-empirical solutions of the Clausius-Clapeyron equation but with different approaches of integration, as well as of boiling temperature evaluation. Camredon's method is considered to underestimate $p^0_{L,i}$, contrary to Jenkin's method which significantly overestimates the vapour pressures. This would translate into overestimation, respectively underestimation of the partitioning coefficients. Yet, both estimations delivered K_p s up to three orders of magnitude lower than the experimental data. Within the instrumental accuracy and precision range only the partitioning coefficient of hydroxynopinone calculated using the Camredon approach is comparable to the observed value.

Overall, it was shown that the K_p theoretical estimations were more sensitive to the vapour pressure calculations, and less sensitive to activity coefficient predictions. Moreover, there are indications, that the absorption equilibrium formalism cannot fully describe the gas-particle partitioning of semi-volatile organic compounds such as nopinone. When using equilibrium partitioning assumption in modeling of the organic matter in the atmosphere, the discrepancy between calculated and measured partitioning coefficients will likely results in underestimation of the predicted amount of semi-volatile organic compounds in secondary organic aerosol. Laboratory experiments to determine partitioning coefficients, such as presented in this work, are needed to gain further insight into the complexity of gas-particle partitioning processes and thus to provide a wider data base for model studies.

Notes

a Forschungszentrum Juelich, Juelich , Germany. Fax: +49 2461 615346; Tel: +49 2461 616930; E-mail: i.gensch@fz-juelich.de
*b Aerodyne Research, Inc., Billerica, USA*

References

1. B. Bonn, G. Schuster and G. K. Moortgat, *J. Phys. Chem. A*, 2002, **106**, 2869-2881.
2. T. Hoffmann, J. R. Odum, F. Bowman, D. Collins, D. Klockow, R. C. Flagan and J. H. Seinfeld, *J. Atmos. Chem.*, 1997, **26**, 189-222.
3. R. J. Griffin, D. R. Cocker, III, J. H. Seinfeld and D. Dabdub, *Geophys. Res. Lett.*, 1999, **26**, 2721-2724.
4. R. J. Griffin, D. Dabdub and J. H. Seinfeld, *J. Geophys. Res., [Atmos.]*, 2002, **107**, AAC3/1-AAC3/26.
5. M. Kanakidou, J. H. Seinfeld, S. N. Pandis, I. Barnes, F. J. Dentener, M. C. Facchini, R. Van Dingenen, B. Ervens, A. Nenes, C. J. Nielsen, E. Swietlicki, J. P. Putaud, Y. Balkanski, S. Fuzzi, J. Horth, G. K. Moortgat, R. Winterhalter, C. E. L. Myhre, K. Tsigaridis, E. Vignati, E. G. Stephanou and J. Wilson, *Atmos. Chem. Phys.*, 2005, **5**, 1053-1123.
6. M. E. Jenkin, S. M. Saunders, V. Wagner and M. J. Pilling, *Atmos. Chem. Phys.*, 2003, **3**, 181-193.
7. N. M. Donahue, S. A. Epstein, S. N. Pandis and A. L. Robinson, *Atmos. Chem. Phys.*, 2011, **11**, 3303-3318.
8. J. F. Pankow, *Atmos. Environ.*, 2003, **37**, 3323-3333.
9. M. Barley, D. O. Topping, M. E. Jenkin and G. McFiggans, *Atmos. Chem. Phys.*, 2009, **9**, 2919-2932.
10. S. O'Meara, A. M. Booth, M. H. Barley, D. Topping and G. McFiggans, *Phys. Chem. Chem. Phys.*, 2014, **16**, 19453-19469.
11. A. H. Goldstein and I. E. Galbally, *Environ. Sci. Technol.*, 2007, **41**, 1514-1521.
12. M. Hallquist, J. C. Wenger, U. Baltensperger, Y. Rudich, D. Simpson, M. Claeys, J. Dommen, N. M. Donahue, C. George, A. H. Goldstein, J. F. Hamilton, H. Herrmann, T. Hoffmann, Y. Iinuma, M. Jang, M. E. Jenkin, J. L. Jimenez, A. Kiendler-Scharr, W. Maenhaut, G. McFiggans, T. F. Mentel, A. Monod, A. S. H. Prevot, J. H. Seinfeld, J. D. Surratt, R. Szmigielski and J. Wildt, *Atmos. Chem. Phys.*, 2009, **9**, 5155-5236.
13. G. McFiggans, D. O. Topping and M. H. Barley, *Atmos. Chem. Phys.*, 2010, **10**, 10255-10272.
14. D. V. Spracklen, J. L. Jimenez, K. S. Carslaw, D. R. Worsnop, M. J. Evans, G. W. Mann, Q. Zhang, M. R. Canagaratna, J. Allan, H. Coe, G. McFiggans, A. Rap and P. Forster, *Atmos. Chem. Phys.*, 2011, **11**, 12109-12136.
15. I. Kourtchev, S. J. Fuller, C. Giorio, R. M. Healy, E. Wilson, I. O'Connor, J. C. Wenger, M. McLeod, J. Aalto, T. M. Ruuskanen, W. Maenhaut, R. Jones, D. S. Venables, J. R. Sodeau, M. Kulmala and M. Kalberer, *Atmos. Chem. Phys.*, 2014, **14**, 2155-2167, 2113 pp.
16. K. Kristensen, K. L. Enggrob, S. M. King, D. R. Worton, S. M. Platt, R. Mortensen, T. Rosenoern, J. D. Surratt, M. Bilde, A. H. Goldstein and M. Glasius, *Atmos. Chem. Phys.*, 2013, **13**, 3763-3776, 3714 pp.
17. A. Jordan, S. Haidacher, G. Hanel, E. Hartungen, J. Herbig, L. Maerk, R. Schottkowsky, H. Seehauser, P. Sulzer and T. D. Maerk, *Int. J. Mass Spectrom.*, 2009, **286**, 32-38.
18. T. Hohaus, D. Trimborn, A. Kiendler-Scharr, I. Gensch, W. Laumer, B. Kammer, S. Andres, H. Boudries, K. A. Smith, D. R. Worsnop and J. T. Jayne, *Atmos. Meas. Tech.*, 2010, **3**, 1423-1436.
19. N. M. Donahue, A. L. Robinson, C. O. Stanier and S. N. Pandis, *Environ Sci Technol*, 2006, **40**, 2635-2643.
20. M. E. Jenkin, *Atmos. Chem. Phys.*, 2004, **4**, 1741-1757.
21. J. F. Pankow, *Atmos. Environ.*, 1994, **28**, 185-188.
22. R. Kamens, M. Jang, C. J. Chien and K. Leach, Aerosol formation from the reaction of alpha-pinene and ozone using a gas phase kinetics-aerosol partitioning model, 1999.
23. J. H. Seinfeld and J. F. Pankow, *Annu Rev Phys Chem*, 2003, **54**, 121-140.
24. M. Camredon, J. F. Hamilton, M. S. Alam, K. P. Wyche, T. Carr, I. R. White, P. S. Monks, A. R. Rickard and W. J. Bloss, *Atmos. Chem. Phys.*, 2010, **10**, 2893-2917.
25. P. B. Myrdal and S. H. Yalkowsky, *Ind. Eng. Chem. Res.*, 1997, **36**, 2494-2499.
26. K. G. Joback and R. C. Reid, *Chem. Eng. Commun.*, 1987, **57**, 233-243.
27. M. H. Barley and G. McFiggans, *Atmos. Chem. Phys.*, 2010, **10**, 749-767.
28. D. Mackay, A. Bobra, D. W. Chan and W. Y. Shiu, *Environ. Sci. Technol.*, 1982, **16**, 645-649.
29. S. E. Stein and R. L. Brown, *J. Chem. Inf. Comput. Sci.*, 1994, **34**, 581-587.
30. T. F. Mentel, J. Wildt, A. Kiendler-Scharr, E. Kleist, R. Tillmann, M. Dal Maso, R. Fisseha, T. Hohaus, H. Spahn, R. Uerlings, R. Wegener, P. T. Griffiths, E. Dinar, Y. Rudich and A. Wahner, *Atmos. Chem. Phys.*, 2009, **9**, 4387-4406.
31. R. Atkinson and J. Arey, *Chem Rev*, 2003, **103**, 4605-4638.
32. M. R. Canagaratna, J. T. Jayne, J. L. Jimenez, J. D. Allan, M. R. Alfarra, Q. Zhang, T. B. Onasch, F. Drewnick, H. Coe, A. Middlebrook, A. Delia, L. R. Williams, A. M. Trimborn, M. J. Northway, P. F. DeCarlo, C. E. Kolb, P. Davidovits and D. R. Worsnop, *Mass Spectrom. Rev.*, 2007, **26**, 185-222.
33. J. T. Jayne, D. C. Leard, X. Zhang, P. Davidovits, K. A. Smith, C. E. Kolb and D. R. Worsnop, *Aerosol Sci. Technol.*, 2000, **33**, 49-70.
34. P. F. DeCarlo, J. R. Kimmel, A. Trimborn, M. J. Northway, J. T. Jayne, A. C. Aiken, M. Gonin, K. Fuhrer, T. Horvath, K. S. Docherty, D. R. Worsnop and J. L. Jimenez, *Anal. Chem.*, 2006, **78**, 8281-8289.
35. B. Langford, P. K. Misztal, E. Nemitz, B. Davison, C. Helfter, T. A. M. Pugh, A. R. MacKenzie, S. F. Lim and C. N. Hewitt, *Atmos. Chem. Phys.*, 2010, **10**, 8391-8412.
36. P. K. Misztal, M. R. Heal, E. Nemitz and J. N. Cape, *Int. J. Mass Spectrom.*, 2012, **310**, 10-19.
37. J. H. Park, A. H. Goldstein, J. Timkovsky, S. Fares, R. Weber, J. Karlik and R. Holzinger, *Atmos. Chem. Phys.*, 2013, **13**, 1439-1456, 1418 pp.
38. J. Zhao and R. Zhang, *Atmos. Environ.*, 2004, **38**, 2177-2185.

39. J. D. Allan, J. L. Jimenez, P. I. Williams, M. R. Alfarra, K. N. Bower, J. T. Jayne, H. Coe and D. R. Worsnop, *J. Geophys. Res., [Atmos.]*, 2003, **108**, AAC1/1-AAC1/10.

40. I. M. Ulbrich, M. R. Canagaratna, Q. Zhang, D. R. Worsnop and J. L. Jimenez, *Atmos. Chem. Phys.*, 2009, **9**, 2891-2918.

41. P. Liu, P. J. Ziemann, D. B. Kittelson and P. H. McMurry, *Aerosol Sci. Technol.*, 1995, **22**, 314-324.

42. P. Liu, P. J. Ziemann, D. B. Kittelson and P. H. McMurry, *Aerosol Sci. Technol.*, 1995, **22**, 293-313.

43. K. Jay and L. Stieglitz, *Product analysis of the chemical/photochemical conversion of monoterpenes with airborne pollutants (ozone/nitrogen dioxide)*, Report 0303-755X, Kernforschungszent. Karlsruhe, 1988.

44. A. C. Aiken, P. F. Decarlo, J. H. Kroll, D. R. Worsnop, J. A. Huffman, K. S. Docherty, I. M. Ulbrich, C. Mohr, J. R. Kimmel, D. Sueper, Y. Sun, Q. Zhang, A. Trimborn, M. Northway, P. J. Ziemann, M. R. Canagaratna, T. B. Onasch, M. R. Alfarra, A. S. H. Prevot, J. Dommen, J. Duplissy, A. Metzger, U. Baltensperger and J. L. Jimenez, *Environ Sci Technol*, 2008, **42**, 4478-4485.

45. N. L. Prisle, G. J. Engelhart, M. Bilde and N. M. Donahue, *Geophys. Res. Lett.*, 2010, **37**, L01802/01801-L01802/01805.

46. A. Zuend, C. Marcolli, A. M. Booth, D. M. Lienhard, V. Soonsin, U. K. Krieger, D. O. Topping, G. McFiggans, T. Peter and J. H. Seinfeld, *Atmos. Chem. Phys.*, 2011, **11**, 9155-9206.

47. V. Perraud, E. A. Bruns, M. J. Ezell, S. N. Johnson, Y. Yu, M. L. Alexander, A. Zelenyuk, D. Imre, W. L. Chang, D. Dabdub, J. F. Pankow and B. J. Finlayson-Pitts, *Proc Natl Acad Sci U S A*, 2012, **109**, 2836-2841.

48. A. Kahnt, Dr. rer. nat. Dissertation, Universität Leipzig, 2012.

49. R. J. Barthelmie and S. C. Pryor, *J. Geophys. Res., [Atmos.]*, 1999, **104**, 23657-23669.

50. J. R. Odum, T. Hoffmann, F. Bowman, D. Collins, R. C. Flagan and J. H. Seinfeld, *Environ. Sci. Technol.*, 1996, **30**, 2580-2585.
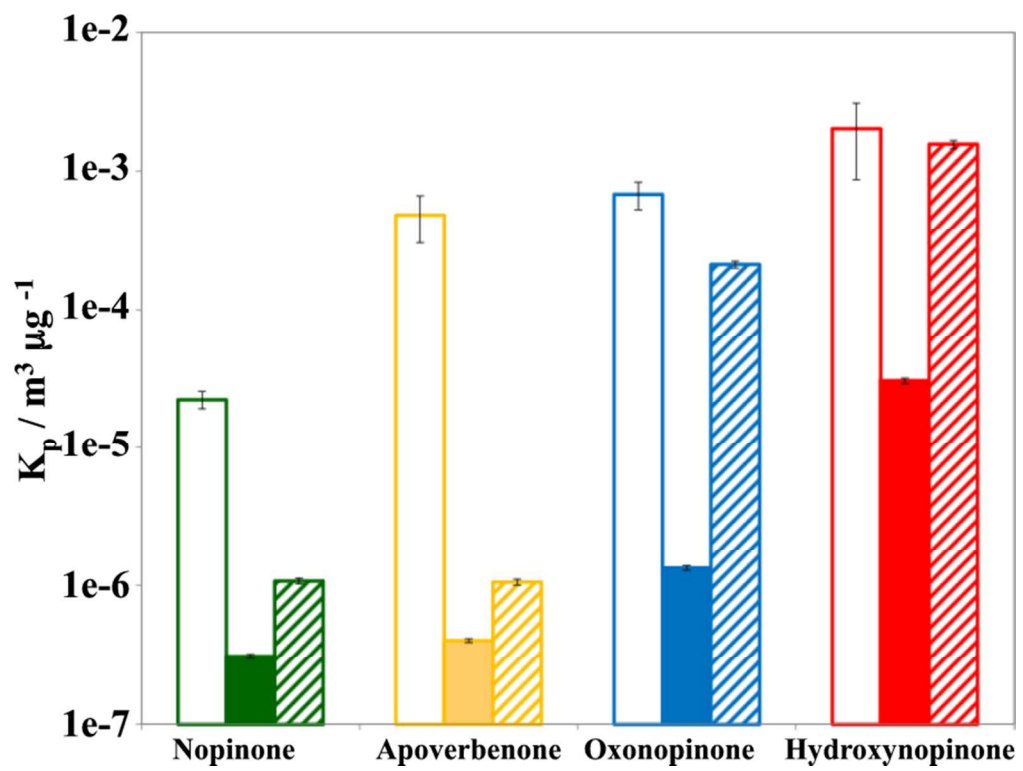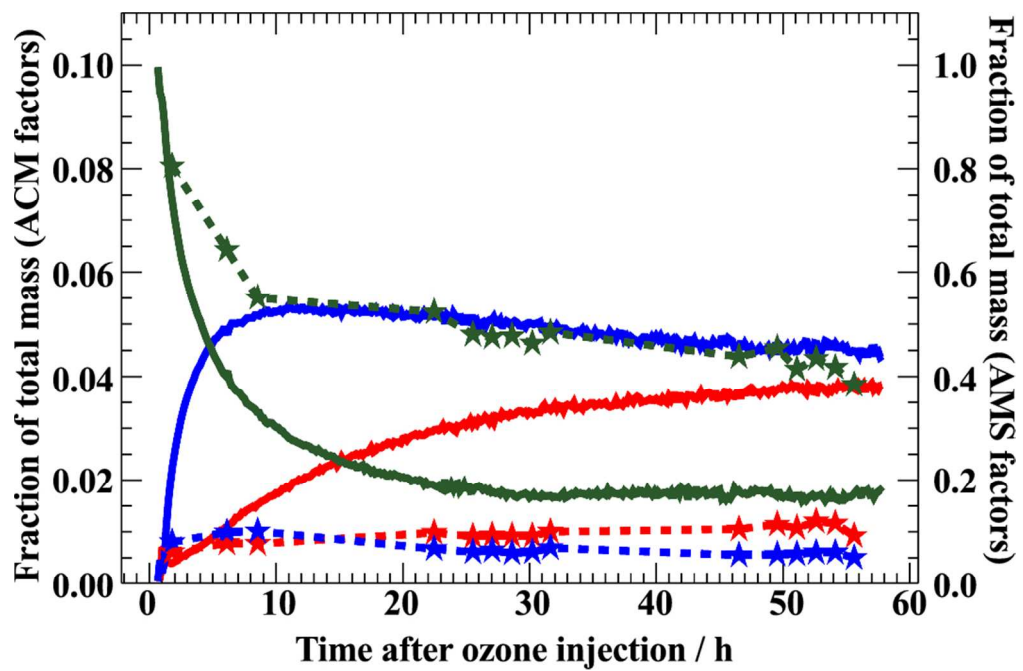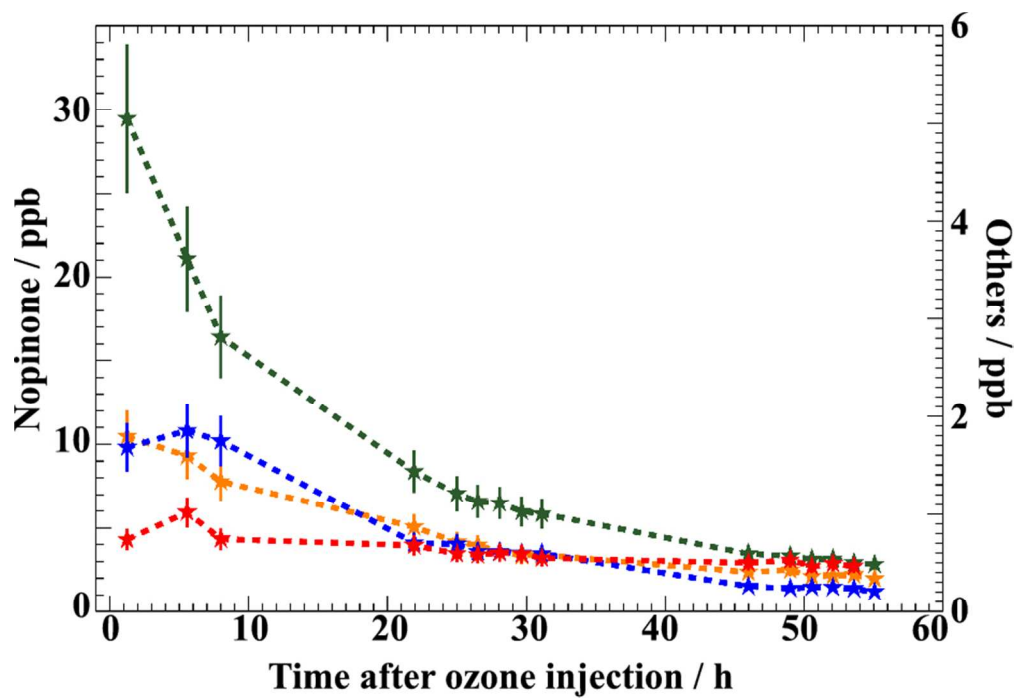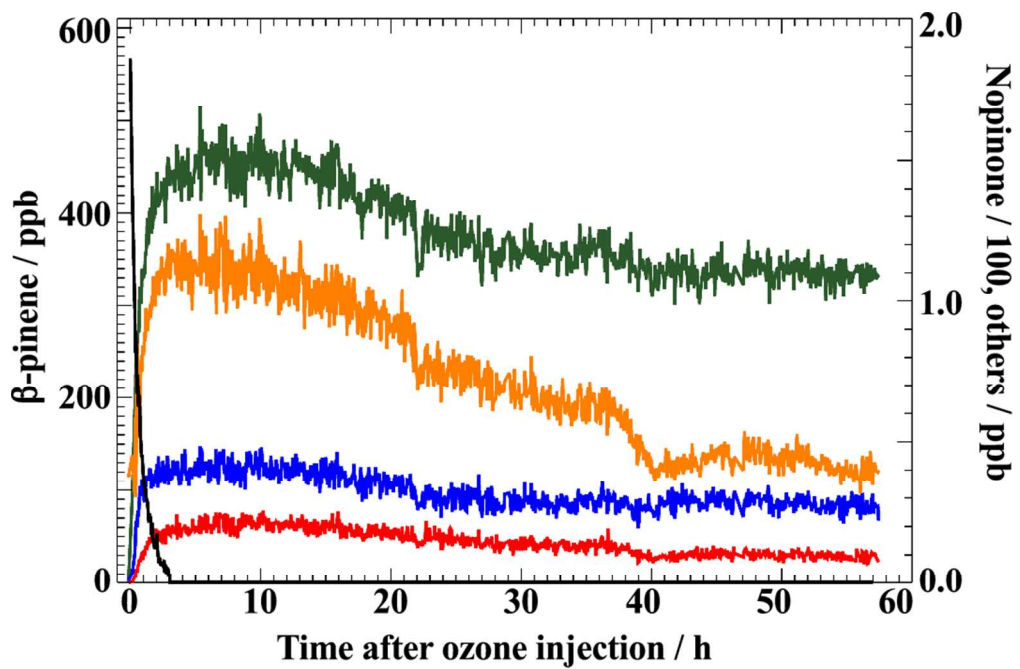
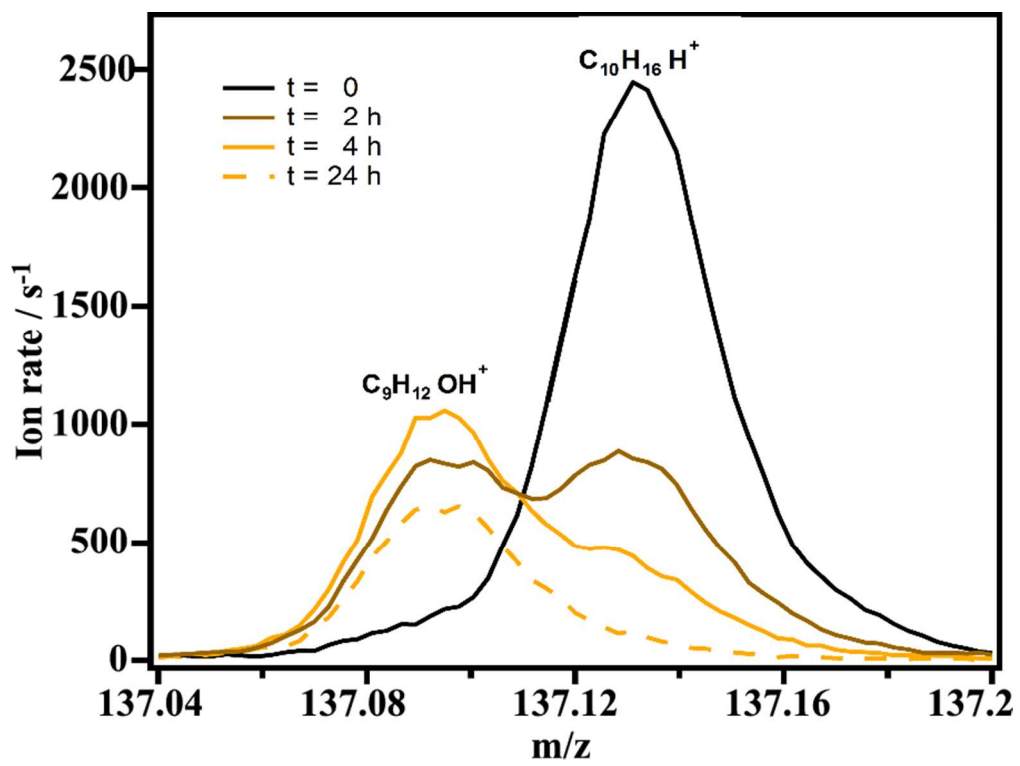237x178mm (96 x 96 DPI)
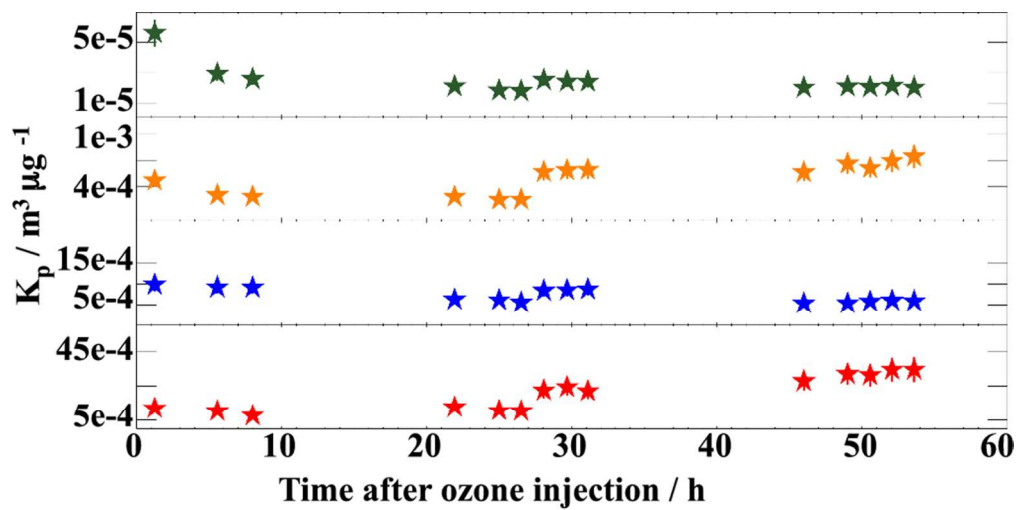
268x133mm (96 x 96 DPI)

280x184mm (96 x 96 DPI)

246x168mm (96 x 96 DPI)

282x185mm (96 x 96 DPI)

238x177mm (96 x 96 DPI)